International Journal of Nanomedicine

Dovepress

open access to scientific and medical research

Open Access Full Text Article

ORIGINAL RESEARCH

Single Atom-Dispersed Silver Incorporated in ZIF-8-Derived Porous Carbon for Enhanced Photothermal Activity and Antibacterial Activities

Yutong Zheng[1], Xiaoyi Cai[1], Gui Chen[1], Dexuan Xiang[1], Wei Shi[1], Jianliang Shen[2], Bailin Xiang[1]

[1]College of Chemistry and Materials Engineering, Huaihua University, Huaihua, 418000, People's Republic of China; [2]State Key Laboratory of Ophthalmology, Wenzhou Medical University, University of Chinese Academy of Sciences, Wenzhou, 325000, People's Republic of China

Correspondence: Bailin Xiang, College of Chemistry and Materials Engineering, Huaihua University, Huaihua, 418000, People's Republic of China, Email xsz96@163.com; Jianliang Shen, State Key Laboratory of Ophthalmology, Wenzhou Medical University, University of Chinese Academy of Sciences, Wenzhou, 325000, People's Republic of China, Email shenjl@wiucas.ac.cn

Purpose: Recently, Single-atom-loaded carbon-based material is a new environmentally friendly and stable photothermal antibacterial nanomaterial. It is still a great challenge to achieve single-atom loading on carbon materials.

Materials and Methods: Herein, We doped single-atom Ag into ZIF-8-derived porous carbon to obtain Ag-doped ZIF-8-derived porous carbon(Ag_{SA}-ZDPC). The as-prepared samples were characterized by XRD, XPS, FESEM, EDX, TEM, and HAADF-STEM which confirmed that the single-atom Ag successfully doped into the porous carbon. Further, the photothermal properties and antimicrobial activity of Ag_{SA}-ZDPC have been tested.

Results: The results showed that the temperature increased by 30 °C after near-infrared light irradiation(1 W/cm^2) for 5 min which was better than ZIF-8-derived porous carbon(ZDPC). It also exhibits excellent photothermal stability after the laser was switched on and off 5 times. When the Ag_{SA}-ZDPC concentration was greater than 50 μg/mL and the near-infrared irradiation was performed for 5 min, the growth inhibition of S. aureus and E. coli was almost 100%.

Conclusion: This work provides a simple method for the preparation of single-atom Ag-doped microporous carbon which has potential antibacterial application.

Keywords: Single-atom, Ag, ZIF-8, photothermal, antibacterial

Introduction

Bacterial infections pose a great threat to human health worldwide.[1,2] At the same time, the challenge of antibiotic resistance is greatly increasing with the abuse of antibiotics.[3–6] It is urgent to exploit new antibiotic-free tactics against rapidly evolving antimicrobial resistance.[7–9]

Photothermal therapy (PTT) was considered an effective method for inhibiting bacterial growth and avoiding antimicrobial resistance.[10–13] Photothermal therapy depends on local heating against bacteria according to the low heat tolerance of ordinary pathogens. There are many nanomaterials used as photothermal antibacterial materials extensively due to the rapid development of nanotechnology, such as semiconductors, precious metals, non-metals, etc.[14–18] Among them, carbon-based material is a good photothermal material because of its high photothermal effect under photoexcitation conditions.[19,20] In particular, carbon-based nanomaterials have the merits of physical and chemical stability, biocompatibility, and environmental friendliness, which make them more application space in the medical field.[21–23] Recently, a high-surface-area carbon-based nanomaterial has been obtained by direct carbonization of Metal-organic framework materials (MOFs) which are characterized by structural designability and huge specific surface area.[24–28] However, how to improve the photothermal properties of carbon-based materials in a proper near-infrared (NIR) range is still a challenge.

Received: 11 January 2024
Accepted: 6 May 2024
Published: 14 May 2024

It was observed that doping a single atom often results in the energy band transition on underlying material and many single-atom doped photothermal antibacterial materials are derived.[29–31] Single-atom catalysis has good catalytic performance due to the fully exposed atomic active metal sites.[32–34] At the same time, Single metal atom doped materials have good potential for biomedical applications due to negligible leakage of metal ions.[35,36] However, it is still a challenge to decorate noble metal atoms onto materials because noble metal nanoparticles with high surface energy are easily agglomerated during the preparation process.[37] Benefiting from the cage-like structure, MOFs can prevent noble metal agglomeration during carbonization.[38] Among MOF materials, ZIF-8 has high thermal and chemical stability and is one of the most studied zeolite imidazolium frameworks (ZIFs). The carbon produced by the carbonization of ZIF-8 at different temperatures still maintains the original structure and morphology.[39,40]

In this paper, Ag ions were first adsorbed into the pores of ZIF-8, and then ZIF-8 was carbonized to obtain single-atom doped porous carbon(Ag_{SA}-ZDPC) (Scheme 1). The incorporation of single-atom Ag is advantageous for enhancing the absorption of near-infrared light and further improving the photothermal conductivity of the material. The photothermal and antibacterial(S. aureus and E. coli) properties of Ag_{SA}-ZDPC were investigated. The results suggested that Ag_{SA}-ZDPC exhibited enhanced photothermal conversion activities and bactericidal performance.

Material and Methods

Materials

2-Methylimidazole ($C_4H_6N_2$), Zinc nitrate hexahydrate ($Zn(NO_3)_2{\cdot}6H_2O$), Methanol (CH_3OH), and Silver nitrate ($AgNO_3$) were all procured from Aladdin Industrial Co., Ltd, Shanghai, China. Tryptic soy broth (TSB), LB Broth (LB), and PBS were procured from Solarbio Industrial, Beijing, China. All aqueous solutions were prepared with deionized water. All chemicals are analytical reagent grade and are used without further purification.

Synthesis of Ag_{SA}-ZDPC

Referring to the synthetic method[41] of the literature. 2-methylimidazole (3.3 g) was completely dispersed in methanol (70 mL) at first. In the second step, $Zn(NO_3)_2{\cdot}6H_2O$ (1.5 g) was dissolved in a methanol (70 mL) solution. Then the two solutions were mixed slowly and stirred at room temperature for 24 hours. The solid product was obtained from the filtration reaction solution washed three times with methanol and vacuum-dried at 80 °C for 24 h. The obtained white solid was ZIF-8.

Dissolve 0.006g of silver nitrate in 10 mL of ethanol, and add 0.2 g of ZIF-8 to the solution. The mixture was filtered after stirring for 1 h. After washing and drying, ZIF-8 adsorbing silver nitrate(Ag/ZIF-8) was obtained. The Ag/ZIF-8 was Carbonized at 900°C for 3h under a nitrogen atmosphere in a tube furnace to obtain Ag-doped ZIF-8-derived porous carbon (Ag_{SA}-ZDPC).

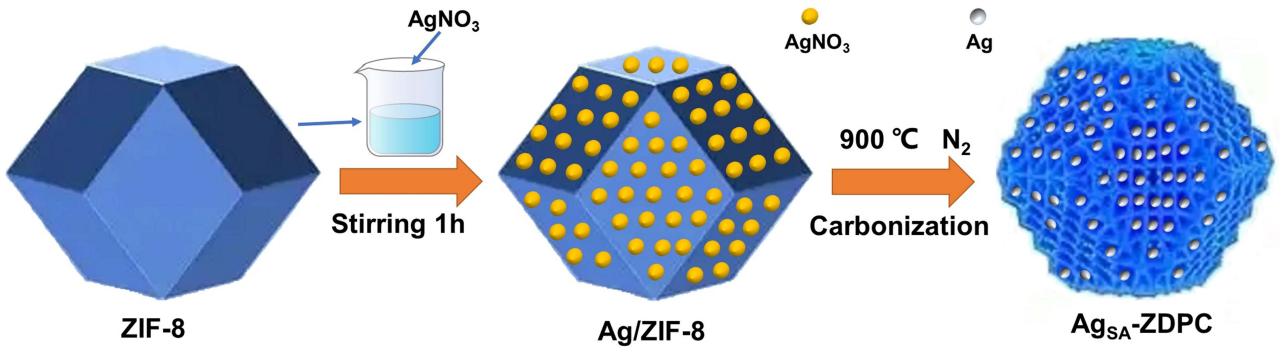

Scheme 1 Schematic illustration of the carbonization of ZIF-8 after adsorption of silver nitrate to obtain single-atom silver-loaded porous carbon(Ag_{SA}-ZDPC).

Characterization

The as-prepared materials were analyzed using the Rigaku Ultima-IV XRD system with Cu-Kα radiation (λ=0.1542 nm) radiation in the range of 5–80°. The morphology of the photocatalyst was observed on a ZEISS Sigma HD field emission scanning electron microscopy (FESEM) with an energy-dispersive X-ray spectroscopy (EDX) analysis. A transmission electron microscopy (TEM) image was taken using a JEOL JEM-2100F UHR transmission electron microscope with an accelerating voltage of 200 kV. X-ray photoelectron spectroscopy (XPS) spectra were obtained via a Thermo Fisher Scientific K-Alpha with Al ka radiation (hν=1486.68 eV). The presence of single atoms was observed using a fifth-order aberration-corrected transmission electron microscope (JEOL ARM200CF). The UV/Vis absorption spectra were obtained using a Metash UV-5500PC spectrophotometer.

Photothermal Performance

The suspension (100 μL) with a certain concentration was illuminated with an 808nm laser (1 W/cm^2) and monitored temperature for 5 minutes. The infrared thermal images of Ag_{SA}-ZDPC under different concentrations of irradiation for 5 min were taken with a Fluke Ti10 infrared camera and recorded every 30 seconds. In the photostability test, the material suspension was irradiated for 5 minutes, then cooled naturally, irradiated 5 times in a cycle, and the temperature was recorded every 30 seconds. The photothermal conversion efficiency (η) of Ag_{SA}-ZDPC was studied by Roper's method.[42]

Antibacterial Activity

Using S. aureus and E. coli as model bacteria, the photothermal sterilization effect of Ag_{SA}-ZDPC in vitro was studied by plate counting method. The bacteria were cultured in TSB or LB in a shaker at 37 °C for 12 h and then dispersed with PBS. The Ag_{SA}-ZDPC suspension (50 μL) in PBS (10, 20, 30, 40, 50, and 75 μg/mL) was mixed with the bacterial solution (50 μL). The mixture was irradiated with a red light at 808 nm for 5 min. After the reaction, the bacterial solution was cultured at 37 °C for 2 hours. Then the bacterial solution was transferred to the agar plate and cultured at 37 °C for 24 hours. The bacterial colonies were photographed and counted for the last time.[43]

Results and Discussion

Characterization

As can be seen from the XRD patterns of ZIF-8 and Ag_{SA}-ZDPC (Figure 1A), the 2θ of diffraction peaks at 7.3°, 10.4°, 12.7°, 14.7°, 16.4°, 18.0°, 22.1°, 24.5 °and 26.7° were ascribed to (011), (002), (112), (022), (013), (222), (114), (233) and (134) planes of ZIF-8.[44] The Ag_{SA}-ZDPC Ag_{SA}-ZDPC's XRD pattern matches amorphous porous carbon due to almost all of the zinc was evaporated at 900 °C in the process of high-temperature carbonization of Ag/ZIF-8 under a nitrogen atmosphere. The characteristic peaks of Ag are inconspicuous illustrating that they were dispersed well in the pores of ZDPC. The chemical states of Ag_{SA}-ZDPC were further characterized by XPS (Figure 1B–D). The survey result in Figure 1B demonstrated peaks attributed to C and Ag, indicating the sample comprised C and Ag elements. Figure 1C was a high-resolution spectra of C. The signal centered at 284.8 was assigned to C-C. The signal centered at 286.4 eV was attributed to C–N Since ZIF-8 contains a small amount of N element. Figure 1D was high-resolution spectra of Ag display that the peaks of 367.8 correspond to Ag 3d5/2 and the 373.8 eV correspond to Ag 3d3/2, showing that Ag doped in Ag_{SA}-ZDPC with the form of metallic silver.[45,46]

The morphologies of ZIF-8 and Ag_{SA}-ZDPC were observed by FESEM (Figure 2A and B). Where Figure 2A displays the FESEM image of ZIF-8. It can be observed that ZIF-8 was spherical particles of uniform size, with a particle size mainly between 40 nm and 50 nm. When ZIF-8 was carbonized, it exhibited a porous morphology with a pore size mainly between 20 nm and 40 nm (Figure 2B). The chemical composition of Ag_{SA}-ZDPC was measured by EDS and mapping (Figure 2C–F), which indicated that the material was mainly composed of C, O, Zn, and Ag (Figure 2C). That is because when Ag/ZIF-8 was carbonized, only C, Ag, and a small amount of O, and Zn remained. The mapping of Ag shows that the Ag nanoparticles supported in Ag_{SA}-ZDPC were distributed well (Figure 2F).

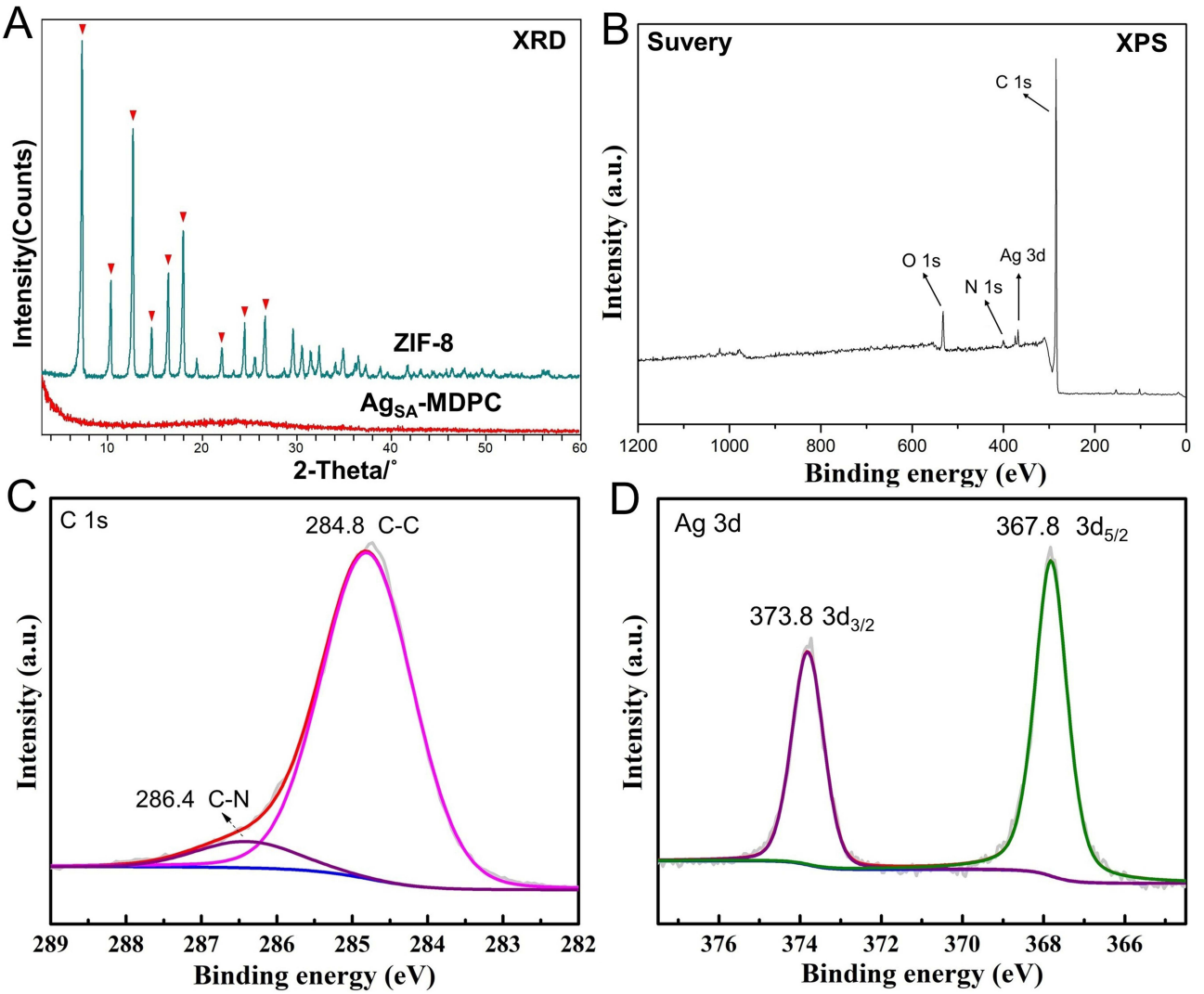

Figure 1 (**A**) XRD patterns of ZIF-8 and Ag_{SA}-ZDPC, XPS spectra of Ag_{SA}-ZDPC: (**B**) survey spectrum, (**C**) C 1s and (**D**) Ag 3d.

TEM images (Figure 3A and B) indicated that the ZIF-8 agglomerated together after carbonization, and exhibited distinct voids and pore structures which correspond to the previous SEM characterization (Figure 2B). From the high-angle annular-dark-field scanning transmission electron microscopy (HAADF-STEM) (Figure 3C and D), it can be found that there are many obvious bright points scattered on the surface of ZDPC, confirming that the atoms of Ag were dispersed on the ZDPC surface (Figure 3D). According to the EDX spectra of the sample, the content of Ag in Ag_{SA}-ZDPC is 0.59 wt% (Figure 2C). The mapping (Figure 2D) also shows that the Ag element was uniformly distributed on the microporous carbon. Combined with the HAADF-STEM image, it can be found Ag particles were successfully deposited on the ZDPC as single atoms.

The Photothermal Effect of Ag_{SA}-ZDPC

UV/Vis spectroscopy was applied to examine the optical behavior of Ag_{SA}-ZDPC and ZDPC. As shown in Figure 4A, the visible and IR light absorption ability of Ag_{SA}-ZDPC is higher than those of ZDPC due to the LSPR of Ag, which is beneficial for photothermal antibacterial applications (vide infra).[47] The photothermal properties of Ag_{SA}-ZDPC were evaluated by recording the temperature changes (Figure 4B–E) under 808 nm laser (1 W/cm^2) irradiation. As shown in Figures 4B and C, the degree of temperature increase is positively correlated with the concentration of Ag_{SA}-ZDPC. The temperature rises of Ag_{SA}-ZDPC solution (50 μg/mL) and ZDPC solution (50 μg/mL) were 30 °C and 12.2 °C,

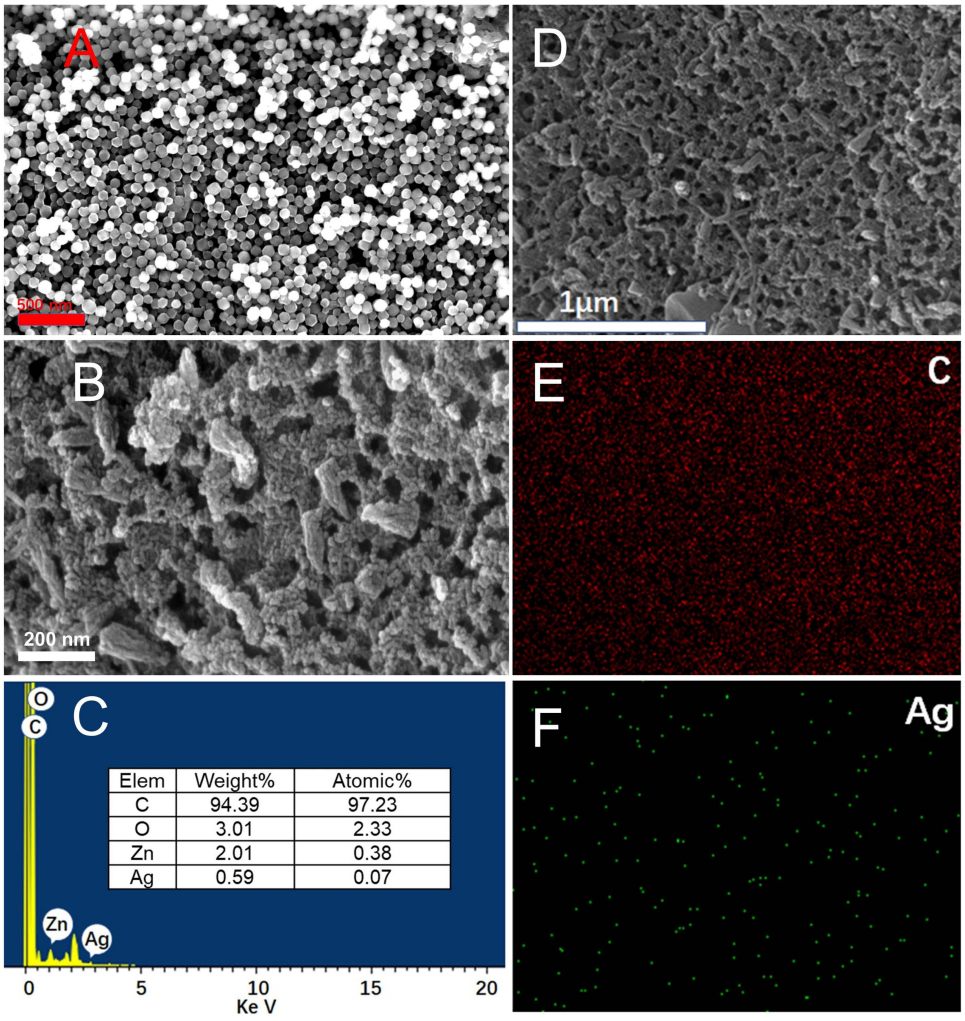

Figure 2 SEM images of (**A**) ZIF-8, (**B**) Ag_{SA}-ZDPC, EDX spectra of (**C**) Ag_{SA}-ZDPC, Mapping of (**D**–**F**) Ag_{SA}-ZDPC.

respectively (Figure 4D) after 5 min of laser irradiation. The results indicated that the incorporation of single-atom Ag in ZDPC can significantly enhance its photothermal conversion through LSPR absorption. Under irradiation at 808 nm, in addition to in-band electron transitions in the ZDPC matrix, Ag absorbs photons which allows more additional electrons to be excited from the valence band and pumped to the conduction band. These extra excited electrons in the conduction band and valence band holes rapidly relax in the metal matrix of the ZDPC and release their energy into the substrate lattice.[48,49] Therefore, the matrix rapidly heats up to a higher temperature than pure ZDPC.[50] The photostability of Ag_{SA}-ZDPC was also evaluated. The samples were irradiated for 5 minutes and then cooled naturally. From Figure 4E, it can be seen that there is no obvious continuous decrease in temperature increase after the laser was switched on and off 5 times, indicating that the Ag_{SA}-ZDPC sample had excellent thermal stability. The linear regression curve of Ag_{SA}-ZDPC (Figure 4F) was obtained from cooling curves according to Roper's report. The photothermal conversion efficiency (η) and the time constant for heat transfer (τ) of Ag_{SA}-ZDPC were calculated to be 28.6% and 78.9 s, respectively.

In vitro Antibacterial Effect of Ag_{SA}-ZDPC

To investigate the photothermal effect of Ag_{SA}-ZDPC on S. aureus and E. coli, the bacteria were processed with different concentrations of Ag_{SA}-ZDPC (0–50 μg/mL) under laser (808 nm, 1W/cm^2) irradiation for 5 min, and then plated on agar plates incubate 24 h at 37 °C, the colonies growing on the agar plates were imaged and counted (Figure 5A–D). It was observed that the viability of the bacteria declined significantly with the rise of the concentration (30 μg/mL −50 μg/mL) of Ag_{SA}-ZDPC under irradiation (Figure 5A–C). The killing rate of S. aureus and E. coli was 99.9% and 100% respectively when the Ag_{SA}-ZDPC

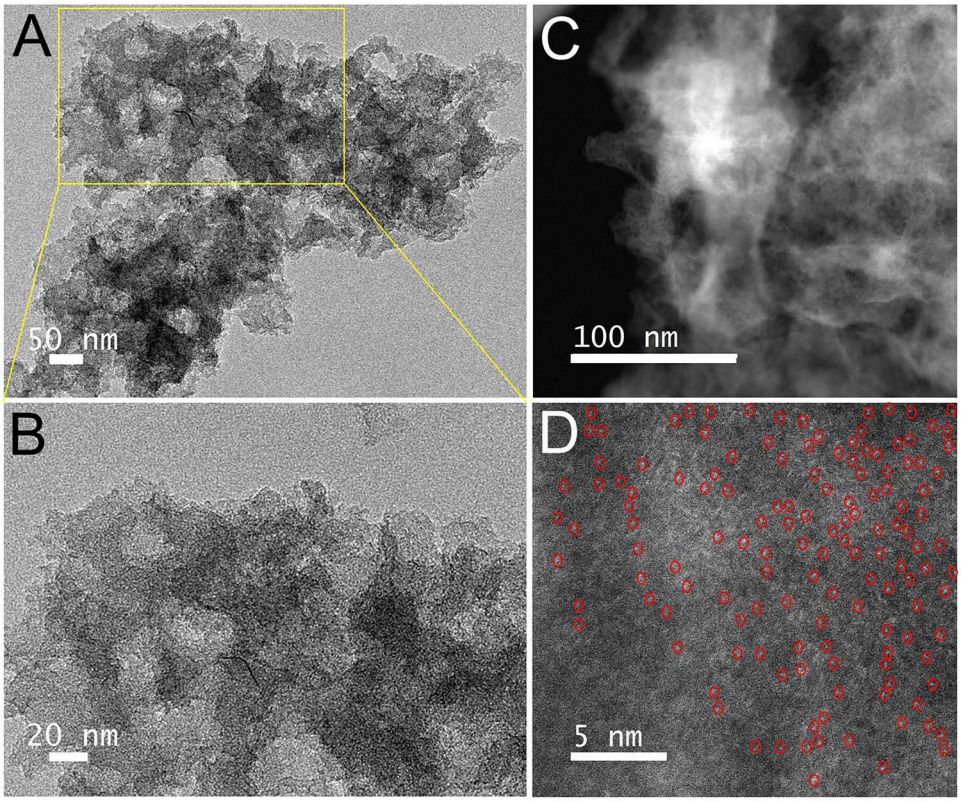

Figure 3 TEM of (**A** and **B**) Ag_{SA}-ZDPC, HAADF-STEM of (**C** and **D**) Ag_{SA}-ZDPC.

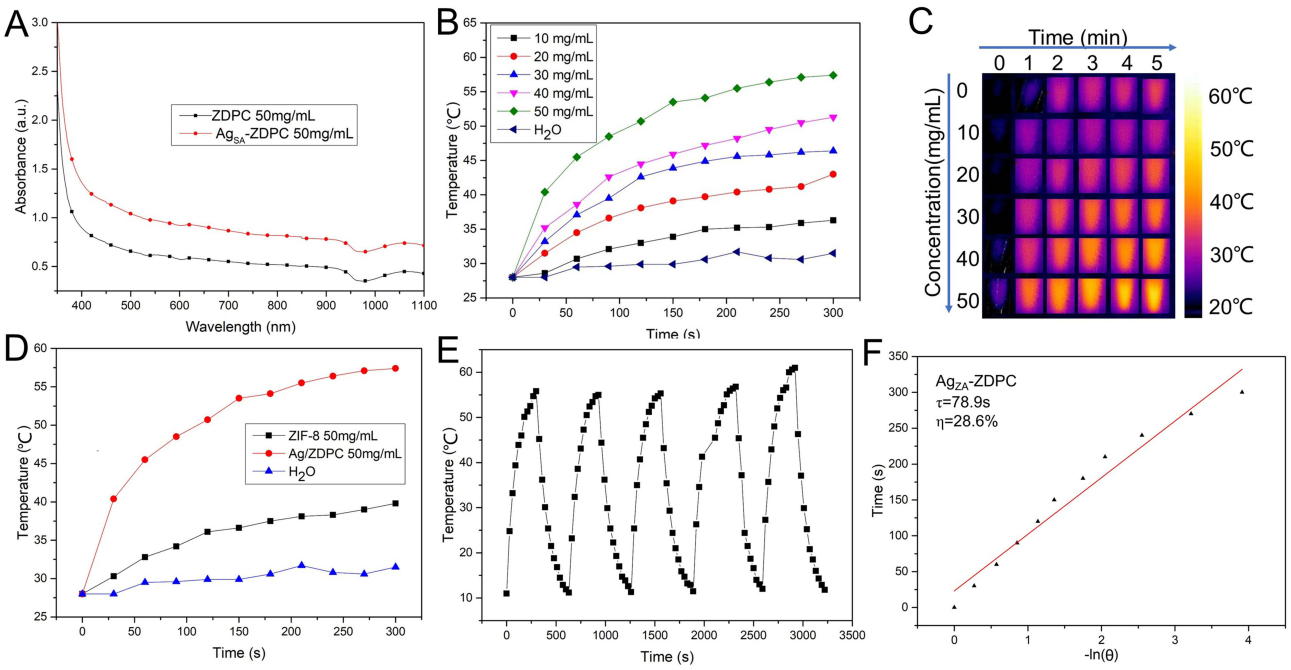

Figure 4 (**A**) UV/Vis absorption of ZDPC and Ag_{SA}-ZDPC, (**B**) Temperature profiles of Ag_{SA}-ZDPC with different concentrations and irradiation time. (**C**) The infrared thermal images of the Ag_{SA}-ZDPC aqueous solution at varying concentrations were taken before and after irradiation using an 808 nm laser (1 W/cm^2). (**D**) Temperature profiles of ZDPC and Ag_{SA}-ZDPC nanocomposites at 50 μg/mL for 300 s via 808 nm laser (1 W/cm^2) irradiation. (**E**) Temperature changes of Ag_{SA}-ZDPC (50 μg/mL) over five cycles using the 808 nm laser (1 W/cm^2). (**F**) Linear regression curve of the cooling part from Ag_{SA}-ZDPC.

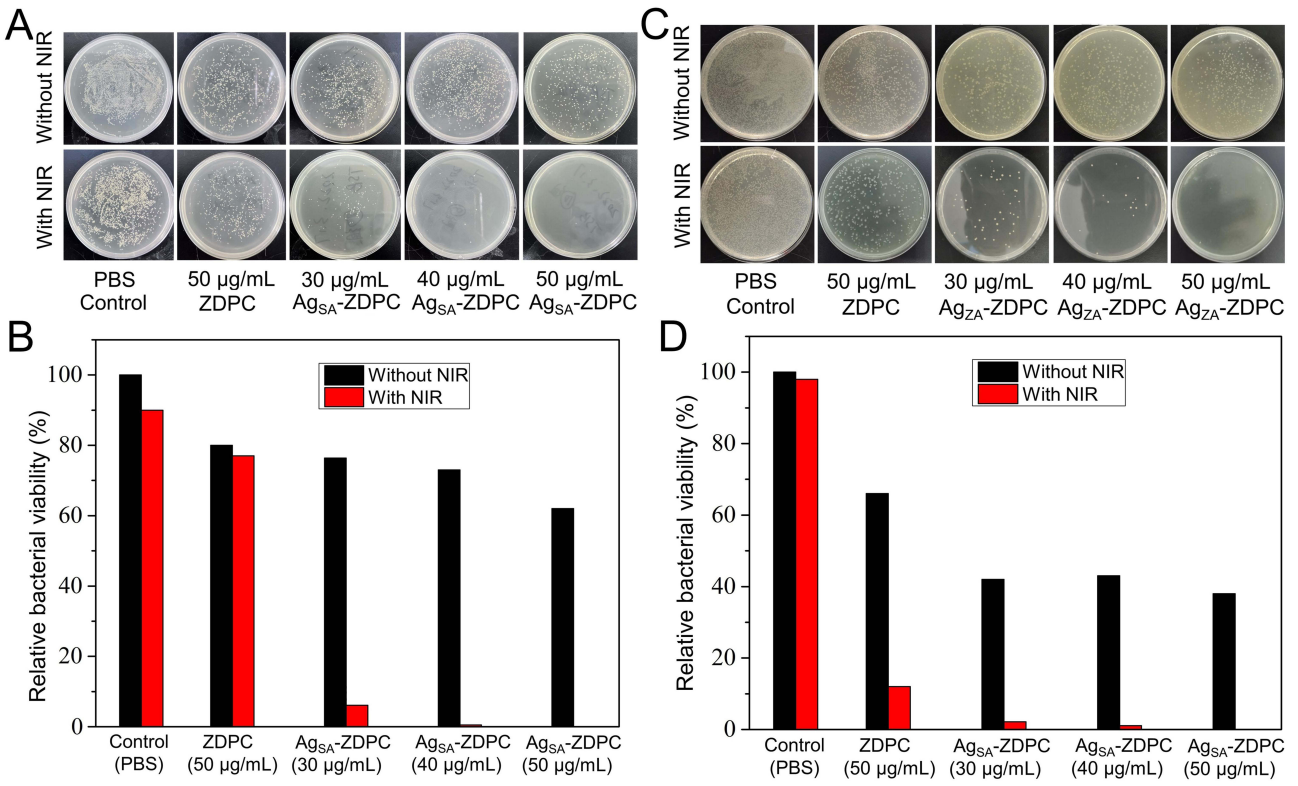

Figure 5 (**A** and **B**) The Relative bacterial viability and (**B** and **D**) photographs of bacterial colonies of (**A** and **B**) S. aureus and (**C** and **D**) E. coli exposed to Ag_{SA}-ZDPC (0–50 μg/mL) at 5 min of NIR irradiation.

concentration was 50 μg/mL with 808 nm laser (1W/cm^2) for 5 min. While the killing rate of S. aureus and E. coli was only 23% and 34% by ZDPC (50 μg/mL) with 808 nm laser (1W/cm^2) for 5 min (Figure 5B–D). The results show that the incorporation of monoatomic Ag greatly improves the bactericidal effect, and the bactericidal effect increases with the increase of Ag_{SA}-ZDPC concentration. In addition, the bacteria treated with Ag_{SA}-ZDPC had a lower mortality rate without near-infrared irradiation, indicating that the Ag_{SA}-ZDPC has less bactericidal activity. This was due to the low concentration of Ag in the Ag_{SA}-ZDPC, which has less effect on inhibiting the growth of bacteria. Monoatomic silver mainly enhances the photothermal effect of ZDPC without enhancing its chemical toxicity.[49] The inhibitory effect of Ag_{SA}-ZDPC on bacteria was due to NIR-induced hyperthermia.

Conclusion

In summary, we synthesized Ag-doped ZIF-8-derived microporous carbon composite, and that confirmed Ag was distributed in the microporous carbon in the form of single atoms verified by XRD, XPS, FESEM, EDX, TEM, and HAADF-STEM. Doping of single-atom Ag on ZIF-8-derived porous carbon maximizes the LSPR of materials in the near-infrared window and improves the photothermal conversion capability. We demonstrated that Ag_{SA}-ZDPC had strong bactericidal activity in vitro, where Ag_{SA}-ZDPC could almost completely kill S. aureus and E. coli under 808 nm laser (1 W/cm^2) irradiation. This work provides a simple method for the preparation of single-atom Ag-doped microporous carbon which has potential antibacterial application.

Acknowledgments

We gratefully acknowledge the support for this research by the scientific research project of the Hunan Engineering Laboratory for Preparation Technology of Polyvinyl Alcohol (PVA) Fiber Material, Huaihua Key Laboratory for preparation of Ceramic Materials and Devices.

Funding

Hunan Provincial Regional Joint Fund (2024JJ7380), Hunan Province Education Department (20C1477), Research Project of Huaihua University (HHUY2019-17), Innovative Training Project for College Students of Hunan Province (S202310548114), Innovative Training Project for College Students of China(202110548015), the Natural Science Foundation of Hunan Province (No. 2021JJ30539).

Disclosure

The authors report no conflicts of interest in this work.

References

1. Pettinari C, Pettinari R, Di Nicola C, Tombesi A, Scuri S, Marchetti F. Antimicrobial MOFs. *Coord Chem Rev*. 2021;446:214121. doi:10.1016/j.ccr.2021.214121
2. Khan SA, Shakoor A. Recent Strategies and Future Recommendations for the Fabrication of Antimicrobial, Antibiofilm, and Antibiofouling Biomaterials. *Int j Nanomed*. 2023;2023(18).
3. Routy B, Chatelier E, Derosa L, CpM D, Daillère M. Gut microbiome influences efficacy of pd-1–based immunotherapy against epithelial tumors. *Science*. 2018;359(6371):91–97. doi:10.1126/science.aan3706
4. Li X, Bai H, Yang Y, Yoon J, Wang S, Zhang X. Supramolecular Antibacterial Materials for Combatting Antibiotic Resistance. *Adv Mater*. 2019;31(5):1805092. doi:10.1002/adma.201805092
5. Fan W, Han H, Lu Z. ε-poly-L-lysine-modified polydopamine nanoparticles for targeted photothermal therapy of drug-resistant bacterial keratitis. *Bioeng Transl Med*. 2022;8(1):1.
6. He X, Koo S, Obeng E, Sharma A, Shen J, Kim JS. Emerging 2D MXenes for antibacterial applications: current status, challenges, and prospects. *Coor Chem Rev*. 2023;492:215275. doi:10.1016/j.ccr.2023.215275
7. Hu B, Owh C, Chee PL, et al. Supramolecular hydrogels for antimicrobial therapy. *Chem Soc Rev*. 2018;47(18):6917–6929. doi:10.1039/C8CS00128F
8. Gupta A, Mumtaz S, Li C-H, Hussain I, Rotello VM. Combatting antibiotic-resistant bacteria using nanomaterials. *Chem Soc Rev*. 2019;48(2):415–427. doi:10.1039/C7CS00748E
9. He X, Qian Y, Wu C, et al. Entropy-Mediated High-Entropy MXenes Nanotherapeutics: NIR-II-Enhanced Intrinsic Oxidase Mimic Activity to Combat Methicillin-Resistant Staphylococcus Aureus Infection. *Adv Mater*. 2023;35(26):2211432. doi:10.1002/adma.202211432
10. Yang Y, Ma L, Cheng C, et al. Nonchemotherapic and robust dual-responsive nanoagents with on-demand bacterial trapping, ablation, and release for efficient wound disinfection. *Adv Funct Mater*. 2018;28(21):1705708. doi:10.1002/adfm.201705708
11. Zhu K, Qian S, Guo H, et al. pH-Activatable Organic Nanoparticles for Efficient Low-Temperature Photothermal Therapy of Ocular Bacterial Infection. *ACS Nano*. 2022;16(7):11136–11151. doi:10.1021/acsnano.2c03971
12. Zhou J, Wang W, Zhang Q, Zhang Z, Guo J, Yan F. Oxygen-supplied mesoporous carbon nanoparticles for enhanced photothermal/photodynamic synergetic therapy against antibiotic-resistant bacterial infections. *Chem. Sci*. 2022;13(23):6967–6981. doi:10.1039/D2SC01740G
13. He X, Hou J-T, Sun X, et al. NIR-II Photo-Amplified Sonodynamic Therapy Using Sodium Molybdenum Bronze Nanoplatform against Subcutaneous Staphylococcus Aureus Infection. *Adv Funct Mater*. 2022;32(38):2203964. doi:10.1002/adfm.202203964
14. Cheng X, Sun R, Yin L, Chai Z, Shi H, Gao M. Light-triggered assembly of gold nanoparticles for photothermal therapy and photoacoustic imaging of tumors in vivo. *Adv Mater*. 2017;29(6):1604894. doi:10.1002/adma.201604894
15. Cheng Y, Chang Y, Feng Y, Jian H, Tang Z, Zhang H. Deep-level defect enhanced photothermal performance of bismuth sulfide–gold heterojunction nanorods for photothermal therapy of cancer guided by computed tomography imaging. *Angew Chem Int Ed*. 2018;57(1):246–251. doi:10.1002/anie.201710399
16. Chen Y, Gao Y, Chen Y, Liu L, Mo A, Peng Q. Nanomaterials-based photothermal therapy and its potentials in antibacterial treatment. *J Control Release*. 2020;328(10):251–262. doi:10.1016/j.jconrel.2020.08.055
17. He X, Dai L, Ye L, et al. A Vehicle-Free Antimicrobial Polymer Hybrid Gold Nanoparticle as Synergistically Therapeutic Platforms for Staphylococcus aureus Infected Wound Healing. *Adv Sci*. 2022;9(14):2105223. doi:10.1002/advs.202105223
18. He X, Lv Y, Lin Y, et al. Platinum Nanoparticles Regulated V_2C MXene Nanoplatforms with NIR-II Enhanced Nanozyme Effect for Photothermal and Chemodynamic Anti-Infective Therapy. *Adv Mater*. 2024;3:2400366. doi:10.1002/adma.202400366
19. Hashemi M, Omidi M, Muralidharan B, et al. Correction to "Evaluation of the Photothermal Properties of a Reduced Graphene Oxide/Arginine Nanostructure for Near-Infrared Absorption". *ACS Appl Mater Inter*. 2017;9(45):39872. doi:10.1021/acsami.7b15455
20. J-W X, Yao K, Z-K X. Nanomaterials with a photothermal effect for antibacterial activities: an overview. *Nanoscale*. 2019;11(18):8680–8691. doi:10.1039/C9NR01833F
21. Karahan HE, Wiraja C, Xu C, et al. Graphene materials in antimicrobial nanomedicine: current status and future perspectives. *Adv Healthcare Mater*. 2018;7(13):1701406. doi:10.1002/adhm.201701406
22. Zhang Y, Wu M, Wu M, Zhu J, Zhang X. Multifunctional Carbon-Based Nanomaterials: applications in Biomolecular Imaging and Therapy. *ACS Omega*. 2018;3(8):9126–9145. doi:10.1021/acsomega.8b01071
23. Rajakumar G, Zhang X-H, Gomathi T, et al. Current use of carbon-based materials for biomedical applications—a prospective and review. *Processes*. 2020;8(3):355. doi:10.3390/pr8030355
24. Chen Y-Z, Zhang R, Jiao L, Jiang H-L. Metal-organic framework-derived porous materials for catalysis. *Coord Chem Rev*. 2018;362:1–23. doi:10.1016/j.ccr.2018.02.008
25. Zhang -N-N, Bigdeli F, Miao Q, M-L H, Morsali A. Ultrasonic-assisted synthesis, characterization and DNA binding studies of Ru(II) complexes with the chelating N-donor ligand and preparing of RuO_2 nanoparticles by the easy method of calcination. *J Organomet Chem*. 2018;878(30):11–18. doi:10.1016/j.jorganchem.2018.09.024

26. Guo H, Xia Y, Feng K, Qu X, Wan FJIJo N. Surface Engineering of Metal-Organic Framework as pH-/NIR-Responsive Nanocarrier for Imaging-Guided Chemo-Photothermal Therapy. *Int j Nanomed*. 2020;15:3235–3250. doi:10.2147/IJN.S239910
27. Rong L. The preparation of metal-organic frameworks and their biomedical application. *Int J Nanomed*. 2016;11:1187–1200. doi:10.2147/IJN.S100877
28. Li Y, Xia X, Hou W, Lv H, Liu J, Li X. How Effective are Metal Nanotherapeutic Platforms Against Bacterial Infections? A Comprehensive Review of Literature. *Int j Nanomed*. 2023;18:1109–1128. doi:10.2147/IJN.S397298
29. Huo M, Wang L, Zhang H, Zhang L, Chen Y, Shi J. Construction of Single-Iron-Atom Nanocatalysts for Highly Efficient Catalytic Antibiotics. *Small*. 2019;15(31):1901834. doi:10.1002/smll.201901834
30. Chang M, Hou Z, Wang M, et al. Single-atom pd nanozyme for ferroptosis-boosted mild-temperature photothermal therapy. *Angew Chem Int Ed*. 2021;60(23):12971–12979. doi:10.1002/anie.202101924
31. Zhu Y, Wang W, Cheng J, et al. Stimuli-responsive manganese single-atom nanozyme for tumor therapy via integrated cascade reactions. *Angew Chem Int Ed*. 2021;60(17):9480–9488. doi:10.1002/anie.202017152
32. Chen Y, Ji S, Wang Y, et al. Isolated single iron atoms anchored on n-doped porous carbon as an efficient electrocatalyst for the oxygen reduction reaction. *Angew Chem*. 2017;129(24):7041–7045. doi:10.1002/ange.201702473
33. Yin Q, Tan L, Lang Q, et al. Plasmonic molybdenum oxide nanosheets supported silver nanocubes for enhanced near-infrared antibacterial activity: synergism of photothermal effect, silver release and photocatalytic reactions. *Appl Catal B*. 2018;224:671–680. doi:10.1016/j.apcatb.2017.11.024
34. Kandathil V, Patil SA. Single-atom nanozymes and environmental catalysis: a perspective. *Adv Colloid Interface Sci*. 2021;294:102485. doi:10.1016/j.cis.2021.102485
35. Xu B, Wang H, Wang W, et al. A single-atom nanozyme for wound disinfection applications. *Angew Chem Int Ed*. 2019;58(15):4911–4916. doi:10.1002/anie.201813994
36. Shi Q, Yu T, Wu R, Liu J. Metal–Support Interactions of Single-Atom Catalysts for Biomedical Applications. *ACS Appl Mater Interfaces*. 2021;13(51):60815–60836. doi:10.1021/acsami.1c18797
37. Zhang M, Wang Y-G, Chen W, et al. Metal (Hydr)oxides@Polymer core–shell strategy to metal single-atom materials. *J Am Chem Soc*. 2017;139(32):10976–10979. doi:10.1021/jacs.7b05372
38. Lee SY, Jang HW, Lee HR, Joh H-I. Size effect of metal–organic frameworks with iron single-atom catalysts on oxygen–reduction reactions. *Carbon Lett*. 2021;31(6):1349–1355. doi:10.1007/s42823-021-00292-9
39. Abbasi Z, Shamsaei E, Leong SK, Ladewig B, Zhang X, Wang H. Effect of carbonization temperature on adsorption property of zif-8 derived nanoporous carbon for water treatment. *Microporous Mesopo Mater*. 2016;236(1):28–37. doi:10.1016/j.micromeso.2016.08.022
40. He Z, Yang H, Gu Y, et al. Green Synthesis of MOF-Mediated pH-Sensitive Nanomaterial AgNPs@ZIF-8 and Its Application in Improving the Antibacterial Performance of AgNPs. *Int j Nanomed*. 2023;18:4857–4870. doi:10.2147/IJN.S418308
41. Jing Y, Wang J, Yu B, et al. A MOF-derived ZIF-8@Zn1−xNixO photocatalyst with enhanced photocatalytic activity. *RSC Adv*. 2017;7(67):42030–42035. doi:10.1039/C7RA08763B
42. Roper DK, Ahn W, Hoepfner M. Microscale heat transfer transduced by surface plasmon resonant gold nanoparticles. *J Phys Chem C*. 2007;111(9):3636–3641. doi:10.1021/jp064341w
43. Zyoud A, Dwikat M, Al-Shakhshir S, et al. Natural dye-sensitized ZnO nano-particles as photo-catalysts in complete degradation of E. coli bacteria and their organic content. *J Photochem Photobiol a Chem*. 2016;328(1):207–216. doi:10.1016/j.jphotochem.2016.05.020
44. Bustamante EL, Fernández JL, Zamaro JM. Influence of the solvent in the synthesis of zeolitic imidazolate framework-8 (ZIF-8) nanocrystals at room temperature. *J Colloid Interface Sci*. 2014;424(15):37–43. doi:10.1016/j.jcis.2014.03.014
45. Wang F, Wang Y, Li Y, et al. The facile synthesis of a single atom-dispersed silver-modified ultrathin g-C_3N_4 hybrid for the enhanced visible-light photocatalytic degradation of sulfamethazine with peroxymonosulfate. *Dalton Trans*. 2018;47(20):6924–6933. doi:10.1039/C8DT00919H
46. Wang K-L, Li Y, Sun T, Mao F, J-K W, Xue B. Ultrafine silver nanoparticles deposited on sodium-doped graphitic carbon nitride towards enhanced photocatalytic degradation of dyes and antibiotics under visible light irradiation. *Appl Surf Sci*. 2019;476(15):741–748. doi:10.1016/j.apsusc.2019.01.168
47. Han P, Mao X, Jin Y, et al. Plasmonic Silver-Nanoparticle-Catalysed Hydrogen Abstraction from the C(sp3)−H Bond of the Benzylic Cα atom for Cleavage of Alkyl Aryl Ether Bonds. *Angew Chem Int Ed*. 2023;62(4):e202215201. doi:10.1002/anie.202215201
48. Chang M, Wang M, Chen Y, Shu M, Zhao Y, Ding B. Self-assembled $CeVO_4$/Ag nanohybrid as photoconversion agents with enhanced solar-driven photocatalysis and NIR-responsive photothermal/photodynamic synergistic therapy performance. *Nanoscale*. 2019;11(20):10129–10136. doi:10.1039/C9NR02412C
49. Yang J, Sun L, Hui S, et al. Ag functionalized SnS_2 with enhanced photothermal activity for safe and efficient wound disinfection. *Biomater Sci*. 2021;9(13):4728–4736. doi:10.1039/D1BM00429H
50. Yang Y, Sun J, Wen J, et al. Single-atom doping in carbon black nanomaterials for photothermal antibacterial applications. *Cell Rep Phy Sci*. 2021;2(8):100535. doi:10.1016/j.xcrp.2021.100535